Preparation of Ni-Based Metal Monolithic Catalysts and a Study of Their Performance in Methane Reforming with CO$_2$

Kai Wang,[a] Xiujin Li,[b] Shengfu Ji,*[a] Bingyao Huang,[a] and Chengyue Li[a]

A series of Ni/SBA-15/Al$_2$O$_3$/FeCrAl metal monolithic catalysts with Ni loadings varying between 3% and 16% were prepared, and their structure was characterized by various techniques. The catalytic activity of the catalyst for methane reforming with CO$_2$ leading to synthesis gas was evaluated using a fixed-bed reactor. The results indicate good catalytic activity of the Ni/SBA-15/Al$_2$O$_3$/FeCrAl samples under the reaction conditions. The catalyst with a Ni loading of 8.0% displays excellent activity and stability at 800°C over 1400 h time on stream. After reaction, the hexagonal mesoporous structure of SBA-15 is still present and the pore walls of SBA-15 prevent the aggregation of nickel. Interactions between NiO, SBA-15, and the Al$_2$O$_3$/FeCrAl support modify the redox properties of the Ni/SBA-15/Al$_2$O$_3$/FeCrAl catalysts.

Introduction

Syngas is an important resource for the chemical industry and is used as a feedstock in many chemical industries to produce methanol and higher hydrocarbons. Nowadays, the principal routes for the conversion of methane into syngas include steam reforming, partial oxidation, and methane reforming with CO$_2$. Relative to steam reforming and partial oxidation, methane reforming with CO$_2$ is a particularly attractive process as it produces synthesis gas with a lower H$_2$/CO ratio, which is suitable for use in Fischer–Tropsch synthesis to generate higher hydrocarbons, and it utilizes CO$_2$, which is considered to be an important greenhouse gas.[1–3] Thus, methane reforming with CO$_2$ to synthesis gas has gained considerable attention in the field of catalysis.[4–6]

Noble metals (Pt, Rh, Ru, Pd) exhibit a good level of activity and selectivity in methane reforming reactions with CO$_2$,[7–9] however, their restricted availability and high cost make them unsuitable for industrial-scale operation. In recent years, supported nickel-based catalysts have attracted increasing interest owing to their similar activity to noble-metal catalysts and low costs. Dissanayake et al.[10] as well as Choudhary et al.[11] reported that the Ni/Al$_2$O$_3$ catalyst led to high methane conversion and good product selectivity in the methane reforming reaction. However, nickel catalysts deactivate quickly because of severe coke deposition. Strategies to prevent the formation of coke include the use of various promoters thereby modifying the acid–base or redox properties of the catalyst. The presence of MgO has been shown to suppress coke formation on the Ni/γ-Al$_2$O$_3$ catalyst. It has also been shown that MgO increases alkalinity and accelerates CH$_4$ activation.[12, 13]

The overall activity and sustainability of the methane reforming reaction can be improved by optimizing the physical and chemical properties of the catalysts and their supports. To enhance metal dispersion and reduce the particle size are considered key to achieving coke-free reforming.[14] Catalysts with well-developed porosity could contribute to greater stability:

Hwang et al.[15] reported that coking was more severe on catalysts with low porosity than on catalysts with high porosity. Though Al$_2$O$_3$ and SiO$_2$ are the most commonly used supports for nickel catalysts, Ni/Al$_2$O$_3$ and Ni/SiO$_2$ are prone to deactivation owing to the sintering of nickel and deposition of carbon.[16] Recently, it was reported that the structures of the support exert an important influence on the catalytic activity of Ni in methane reforming with CO$_2$.[17, 18] Wei et al.[19] reported that Ni supported on nanosized ZrO$_2$ (15–25 nm), MgO (10–20 nm), or γ-Al$_2$O$_3$ (5–19 nm) were highly active and stable. Hwang et al.[15] reported that mesoporous clay-supported Ni catalysts exhibited high activity and a long lifetime of stability. The intensity of the interactions between the metal and support also has an important effect on carbon deposition on the active surface. The weak interaction with the support may increase the sintering and carbon formation.[20–24] Therefore, it is essential to search for new carriers capable of developing strong interactions with the loaded metal.

The newly discovered SBA-15 mesoporous silica material offers potential as a versatile support. Previously,[25] we prepared a Ni/SBA-15 catalyst by wet impregnation which showed good catalyst activity in the methane reforming reaction with CO$_2$. Recently, monolithic catalysts, especially those that use the metal as catalyst support, have gained considerable atten-

[a] K. Wang, Prof. Dr. S. Ji, B. Huang, Prof. C. Li
State Key Laboratory of Chemical Resource Engineering
Beijing University of Chemical Technology
15 Beisanhuan Dong Road, P.O. Box 35, Beijing, 100029 (China)
Fax: (+86)10-6441-9619
E-mail: jisf@mail.buct.edu.cn

[b] Prof. Dr. X. Li
Department of Environmental Engineering
Beijing University of Chemical Technology
15 Beisanhuan Dong Road, Beijing, 100029 (China)

Supporting information for this article is available on the WWW under http://www.chemsuschem.org or from the author.

tion.[26–28] Such catalysts can provide some suitable order flow channels in many forms according to the reactor type and can even be made into monolithic catalytic reactors with honeycomb structure. A comparison of conventional fixed-bed reactors with pellet or powder catalysts shows that those using metallic monolithic catalysts display lower pressure drops, smaller sizes of reactor, and lower temperature gradients.[29,30] Metallic monolithic catalysts have a promising application for reactions with high space velocity and heat effect, such as methane reforming to syngas.

In recent years, there has been considerable research carried out concerning FeCrAl metallic supports for the preparation of structured catalysts. Generally, Al_2O_3 is first deposited onto the metal support as the first wash coat layer,[31,32] and then the active component of the catalyst is introduced onto the surface of the support. Yin et al.[26,33,34] prepared methane combustion catalysts using FeCrAl as support which showed good catalytic activity. To the best of our knowledge, catalysts using FeCrAl as support have not been reported for the methane reforming reaction. Here, we report the preparation and characterization of $Ni/SBA-15/Al_2O_3/FeCrAl$ monolithic catalysts and evaluate their catalytic activity and stability for the methane reforming reaction with CO_2.

Results and Discussion

Characterization of the Catalysts

The X-ray diffraction (XRD) patterns of the FeCrAl metal support and $Ni/SBA-15/Al_2O_3/FeCrAl$ catalysts 1–7 (Table 1) are presented in Figure 1. To understand better the structure of the samples, the phase structures of SBA-15 and Ni/SBA-15 were measured by XRD and the patterns for SBA-15 and 8% Ni/SBA-15 samples are shown (Figure 1 a, b). In the XRD pattern of the support, the characteristic peaks for FeCr are observed at $2\theta =$ 44.3° and 64.6° (JCPDS 34-0396, Figure 1 c). After heat treatment of the support at 950 °C for 15 h, additional peaks are observed ($2\theta = 25.5°$, 35.0°, 37.6°, 43.2°, 52.4°, 57.3°, 66.3°, and 68.0°; Figure 1 d) which suggest that α-Al_2O_3 (JCPDS 88-0826) is formed on the FeCrAl surface as a result of oxidation of aluminum. At the same time, the peak intensity of FeCr decreases, in agreement with previous reports.[31] The formation of the α-Al_2O_3 layer can improve the combination ability between the Al_2O_3 wash coat layer and the FeCrAl support.[31,32] The characteristic peaks for γ-Al_2O_3 ($2\theta = 36.9°$, 45.4°, and 67.5°) are ob-
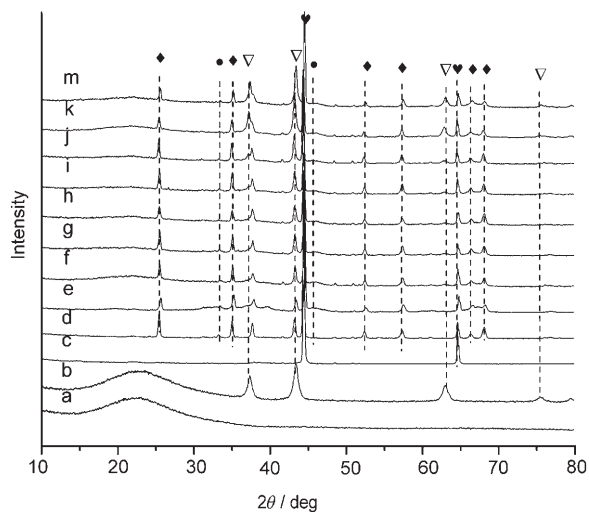

Figure 1. XRD patterns of a) SBA-15, b) 8% Ni/SBA-15, c) FeCrAl, d) FeCrAl pre-oxidized at 950 °C, e) Al_2O_3/FeCrAl, f) catalyst **1**, g) catalyst **2**, h) catalyst **3**, i) catalyst **4**, j) catalyst **5**, k) catalyst **6**, and m) catalyst **7**. Phases: α-Al_2O_3 ($\blacklozenge$); γ-Al_2O_3 ($\bullet$); NiO ($\triangledown$); FeCr (hearts).

served upon coating the FeCrAl support with a slurry of γ-Al_2O_3 (Figure 1 e). Also, the peaks for γ-Al_2O_3 are broader which suggests that γ-Al_2O_3 is finely dispersed on the surface of the FeCrAl support.

For the catalysts **1–7**, the characteristic peaks for NiO(101), NiO(102), NiO(110), and NiO(113) (JCPDS 78-0643) can be clearly seen at $2\theta = 37.2°$, 43.1°, 62.8°, and 75.3°, respectively, for samples with over 4.0% Ni content (catalysts **3–7**; Figure 1 h–m), whereas no characteristic peaks for the NiO phase can be observed with samples that have less than 4.0% Ni content (catalysts **1**, **2**; Figure 1 f, g). The observed results are in good agreement with previous reports.[35] For the Ni/SBA-15 powder, the peaks are sharp and intense, suggesting that the particles of bulk NiO are also larger. This result indicates that the dispersion of nickel is enhanced remarkably when the Ni/SBA-15 powders are deposited onto the surface of the FeCrAl support. Furthermore, the intensity of the NiO peaks increases gradually with increasing Ni content in the $Ni/SBA-15/Al_2O_3/FeCrAl$ series.

The small-angle XRD patterns of SBA-15 and catalysts **1–7** are presented in Figure 2. The diffraction peaks at $2\theta \approx 0.90°$, 1.4°, and 1.7° are ascribed to the hexagonal regularity of the porous structure of SBA-15. This indicates that the hexagonal mesoporous structure of SBA-15 is still present in the $Ni/SBA-15/Al_2O_3/FeCrAl$ catalysts. However, the (100) diffraction peak for the $Ni/SBA-15/Al_2O_3/FeCrAl$ samples shifts to higher 2θ values relative to that of SBA-15, which may be attributed to the constriction of their framework with increasing Ni content during calcination. This phenomenon was also observed by Liu et al.[36] on the V/SBA-15 catalyst. Additionally, a gradual attenuation in the intensity of the (100) peak is observed with increasing Ni content and may be accounted for by considering that partial blocking of the hexagonal pore walls of the SBA-15 materials occurs upon introduction of nickel, especially when the nickel content is very high.[37]

Table 1. Compositions of the catalysts.

Catalyst	Composition
1	3% $Ni/SBA-15/Al_2O_3/FeCrAl$
2	3.5% $Ni/SBA-15/Al_2O_3/FeCrAl$
3	4% $Ni/SBA-15/Al_2O_3/FeCrAl$
4	5% $Ni/SBA-15/Al_2O_3/FeCrAl$
5	8% $Ni/SBA-15/Al_2O_3/FeCrAl$
6	12% $Ni/SBA-15/Al_2O_3/FeCrAl$
7	16% $Ni/SBA-15/Al_2O_3/FeCrAl$
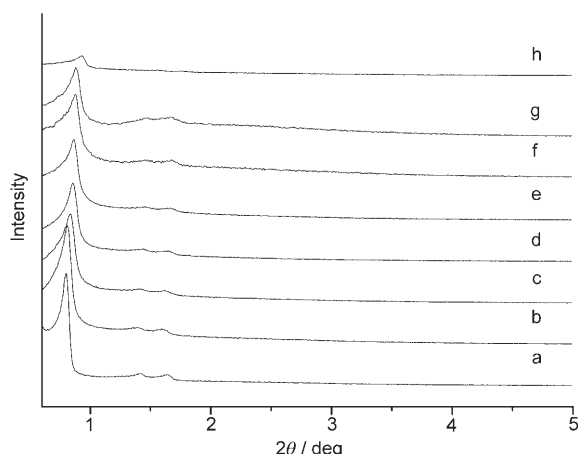
Figure 2. XRD patterns of a) SBA-15, b) catalyst **1**, c) catalyst **2**, d) catalyst **3**, e) catalyst **4**, f) catalyst **5**, g) catalyst **6**, and h) catalyst **7**.
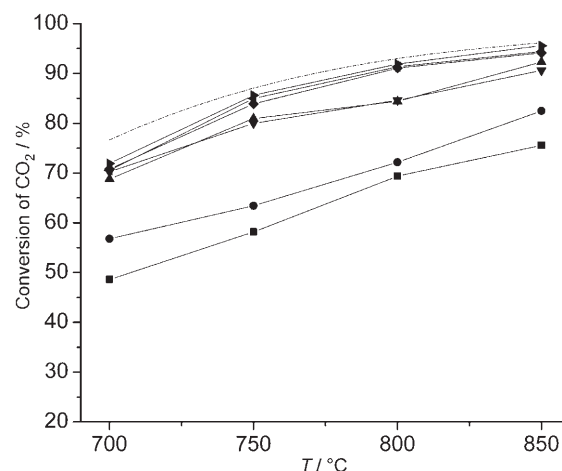

Figure 4. CO_2 conversion over catalysts **1** (■), **2** (●), **3** (▲), **4** (▼), **5** (◆), **6** (◄), and **7** (►); theoretical maximum (–·–·).

Catalyst Activity and Stability

The catalytic performance of samples **1–7** in the methane reforming reaction with CO_2 were studied at atmospheric pressure at reaction temperatures of 700–850 °C with a CH_4/CO_2 ratio of 1.0 and a gas hourly space velocity (GHSV) of 20 000 mL g^{-1} h^{-1}. The influence of temperature on the conversions of methane and carbon dioxide in the reaction over catalysts **1–7** is shown in Figure 3 and Figure 4, respectively. The theoretical (maximum) conversions of CO_2 and CH_4 and selectivities for CO and H_2 are also shown in Figure 3 and Figure 4 as dashed lines (see also the Supporting Information).

From Figure 3 and Figure 4, it is seen that the conversions of CH_4 and CO_2 increase with increasing reaction temperature. Under the same reaction conditions, catalysts **1** and **2** lead to low conversions of CH_4 and CO_2. With increasing nickel content, the catalytic activity increases. When the nickel content is above 4.0 %, the conversions of CH_4 and CO_2 clearly increase. Yan et al.[38] reported a similar result when the nickel content was increased from 7 % to 8 % for a Ni/SiO$_2$ catalyst for methane reforming with CO_2. The accumulation of metal active sites

and the formation of a crystal phase over the catalyst with higher metal content may be responsible for the significant increase in activity of catalysts with high metal loadings. This may be a good indication that an appropriate microstructure is formed when the nickel content is above 4 % in the Ni/SBA-15/Al$_2$O$_3$/FeCrAl catalysts. Upon increasing the nickel content from 8.0 % to 16 % (from **5** to **7**), there is only slight increase in catalytic activity. With catalyst **7**, the CH_4 conversion increases from 73.5 % to 94.5 % while the CO_2 conversion increases from 71.9 % to 95.6 % with a rise in reaction temperature from 700 °C to 850 °C. As compared with previously prepared Ni/SBA-15 catalysts,[25] the conversions CH_4 and CO_2 are all somewhat higher with the present catalysts.

The reaction temperature has little influence on the CO selectivity (see Supporting Information). Under otherwise similar reaction conditions, the selectivity for CO increases with increasing nickel content in the catalysts. The catalyst with the best selectivity for CO is **6** with a loading of 12 % Ni. A further increase in the nickel content leads to a slight drop in the CO selectivity. The selectivity for H_2 increases with increasing nickel content in the temperature range 700–750 °C. However, at temperatures above 800 °C the nickel content has little influence on the H_2 selectivity, which exceeds 97.0 % at 850 °C for all catalysts (see Supporting Information).

The influence of the space velocity on the CH_4 and CO_2 conversions and CO and H_2 selectivities was tested over catalyst **5** at 800 °C at atmospheric pressure with a CH_4/CO_2 ratio of 1.0 (see Supporting Information). As the space velocity increased, the conversion of the CH_4 and CO_2 decreased and the selectivity of the CO and H_2 also dropped slightly. This could be a result of a decrease in the contact time of the reactants and the surface of the catalyst, that is, reaction of the reactants on the surface of the catalyst is not complete and therefore the catalytic activity decreases with higher space velocity. The best conversions of CH_4 and CO_2 were 92.5 % and 91.8 %, respectively, at GHSV = 20 000 mL g^{-1} h^{-1}. At a space velocity of 60 000 mL g^{-1} h^{-1}, the conversions of CH_4 and CO_2 were 82.2 %
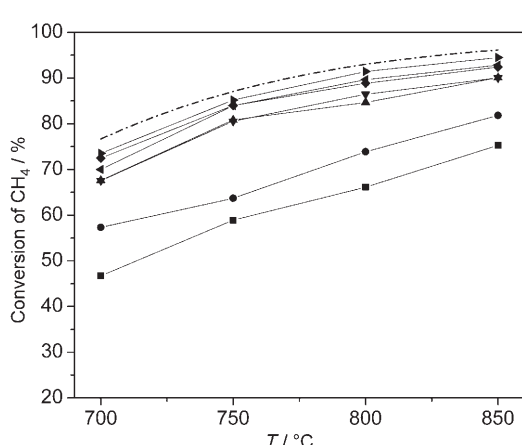

Figure 3. CH_4 conversion over catalysts **1** (■), **2** (●), **3** (▲), **4** (▼), **5** (◆), **6** (◄), and **7** (►); theoretical maximum (–·–·).

and 83.5%, respectively, with selectivities for CO and H_2 of 86.2% and 86.0%, respectively.

From the above results, there is only a slight increase in the catalytic activity with an increase in Ni loading from 8.0% (**5**) to 16% (**7**). Thus, catalyst **5** was selected for study in stability tests. The relationship between the catalytic activity and stability of catalyst **5** at 800°C in the methane reforming reaction with CO_2 is shown in Figure 5. The catalyst was stable over
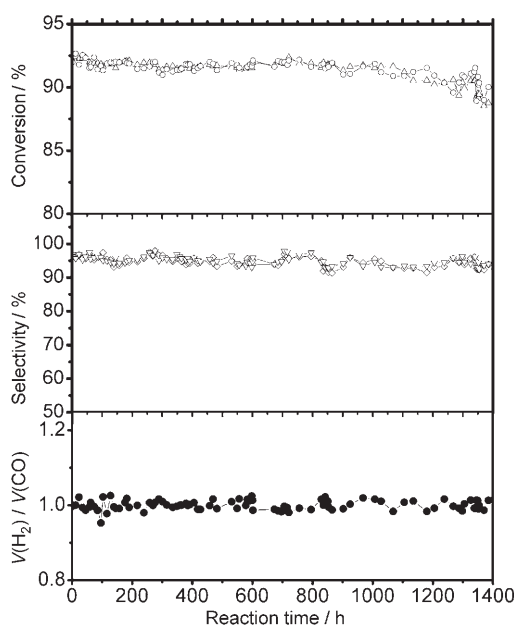

Figure 5. Stability of catalyst **5** at GHSV = 20000 mL g^{-1} h^{-1}, T = 800°C, and $V(CH_4)/V(CO_2)$ = 1. From top to bottom: conversion of CH_4 ($\triangle$) and CO_2 ($\bigcirc$); selectivity for H_2 ($\triangledown$) and CO ($\diamond$); $V(H_2)/V(CO)$ ($\bullet$).

1400 h and displayed good activity under the reaction conditions (T = 800°C, GSHV = 20000 mL g^{-1} h^{-1}, CH_4/CO_2 = 1). The conversions of CH_4 and CO_2 dropped from 92.4% and 92.1%, respectively, to 88.6% and 89.0%, respectively, with time. The selectivities for CO and H_2 decreased over the same period of time from 96.8% and 96.9%, respectively, to 92.3% and 93.6%, respectively. In a previous study,[25] after reaction during 710 h using a Ni/SBA-15 catalyst the conversion of CH_4 decreased by approximately 50% whereas that of CO_2 decreased by approximately 25%. Therefore, in the present case, the FeCrAl support may play a role in stabilizing the Ni/SBA-15/Al$_2$O$_3$/FeCrAl catalyst.

Also note that the molar ratio of H_2 to CO varies between 0.96 and 1.1 during the reaction period. Wei et al.[39] ascribed this phenomenon to a periodic cycle of carbon deposition and elimination. In the present study, the content of coke is 3.9% as shown by the mass increment between the fresh catalyst and the used catalyst after reaction for 1400 h. An efficient periodic cycle of carbon deposition and elimination on the catalyst surface may contribute to the low carbon deposition and stable catalytic performance.

For good stability of the Ni/SBA-15/Al$_2$O$_3$/FeCrAl catalysts, except the main contribution of the FeCrAl support and

carbon deposition and elimination, mesoporous SBA-15 offers many advantageous characteristics as the support relative to conventional silica and alumina supports. The dissolution of NiO in the bulk SBA-15 material results in some difficulty in reducing NiO to Ni. This provides a relatively small amount of segregated small Ni particles on the surface of the support and as a result little sintering occurs. The low sintering is probably even compensated for by some NiO dissolved in SBA-15 which, upon reduction by the hydrogen generated in the reaction, segregates at the solid–gas interface. In this manner, conservation of the exposed surface of Ni is probably achieved. Consequentially, the Ni/SBA-15/Al$_2$O$_3$/FeCrAl catalysts display excellent catalytic activity and stability in the methane reforming reaction with CO_2.

The intrinsic activation energies of the catalysts for the consumption of CH_4 and CO_2 (15.02 kcal mol^{-1} and 16.65 kcal mol^{-1}, respectively) were calculated based on the data of the intrinsic reaction rate–temperature relation. The intrinsic activation energies are lower than those reported for a 6.8% Ni/SiO$_2$ catalyst[40] (23 kcal mol^{-1} for CH_4 and 19 kcal mol^{-1} for CO_2). (Related experimental data and results of calculations are provided in the Supporting Information.)

The XRD patterns of the fresh, reduced, and used catalyst **5** are shown in Figure 6. For the three samples, one major characteristic peak of SBA-15 at about 0.84°–1.0° is observed. The
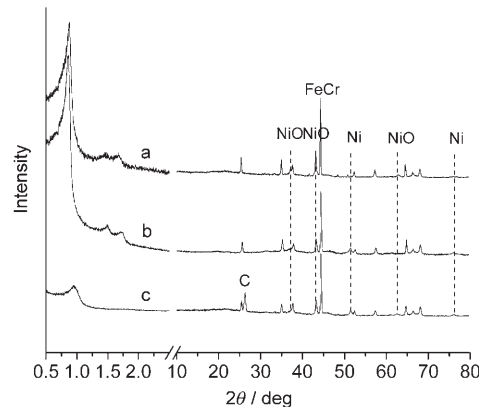

Figure 6. XRD patterns for catalyst **5**: a) fresh sample; b) after reduction at 750°C for 3.5 h; and c) after reaction at 800°C for 1400 h.

results suggest that the pore structure of SBA-15 is retained in the reduced and used catalysts. However, the peak intensity of the used catalyst decreases and the position of the peak shifts to a higher 2θ value relative to that for the fresh catalyst. This indicates that the mesoporous structure of the used catalyst is partly changed after 1400 h reaction. In the XRD profiles of the reduced and used catalysts, peaks corresponding to NiO and Ni appear, suggesting that some Ni is oxidized to NiO during the reaction. This is similar to reported results.[44] Moreover, a peak corresponding to deposited carbon is observed, suggesting that deactivation of catalyst **5** after 1400 h reaction could be caused by coking.

Textural Properties

The characteristics of the pore structures of the fresh, reduced, and used catalyst **5** are shown in Figure 7 and listed in Table 2. All the catalysts show a type IV isotherm and a clear H1-type
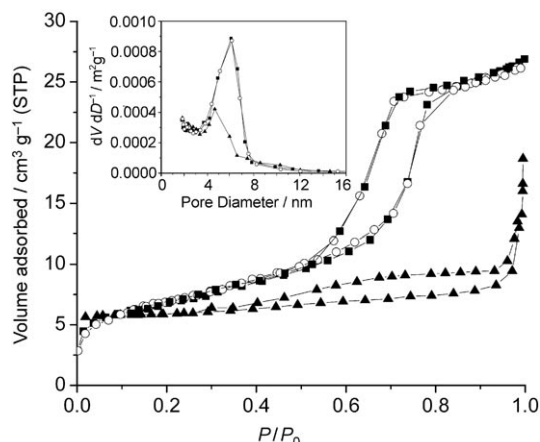

Figure 7. Nitrogen sorption isotherms for catalyst **5**: fresh sample (■); after reduction at 750 °C for 3.5 h (○); and after reaction at 800 °C for 1400 h (▲).

Table 2. Characteristics of catalyst **5**.

Catalyst	A_{BET} [m^{2}g^{-1}][a]	V_{BJH} [cm^{3}g^{-1}][b]	D_{BJH} [nm][c]
5 (fresh)	24.9	0.039	6.05
5 (reduced)[d]	26.1	0.042	6.11
5 (used)[e]	11.7	0.021	4.64

[a] Specific surface area determined by the Brunauer–Emmett–Teller (BET) method. [b] Total pore volume determined by Barrett–Joyner–Halenda (BJH) method. [c] Pore diameter determined by BJH method. [d] After reduction at 750 °C for 3.5 h. [e] After reaction at 800 °C for 1400 h.

hysteresis loop.[42] The fresh catalyst **5** displays a pore diameter (D_{BJH}) of 6.05 nm, a total pore volume (V_{BJH}) of 0.039 cm^{3}g^{-1}, and a BET specific surface area (A_{BET}) of 24.9 m^{2}g^{-1}. The nitrogen adsorption–desorption isotherm of the reduced catalyst is nearly unchanged compared to the fresh catalyst, with $V_{BJH} = 0.041$ cm^{3}g^{-1} and $A_{BET} = 26.1$ m^{2}g^{-1}. The hysteresis loop of the used catalyst **5** exhibits deformation and the adsorbed volume is clearly decreased as compared to the fresh and reduced catalysts, with $D_{BJH} = 4.64$ nm, $V_{BJH} = 0.021$ cm^{3}g^{-1}, and $A_{BET} = 11.7$ m^{2}g^{-1}. This may be due to the fact that coke deposits block the mesochannels and some collapse of pore walls occurs during the reaction. However, the hexagonal mesoporous structure is also present in the used catalyst. The results confirm the relatively well-resolved reflection peaks recorded by XRD (Figure 6).

Redox Properties

The reducibility of the catalysts was characterized by H$_2$ temperature-programmed reduction (TPR) experiments. Figure 8
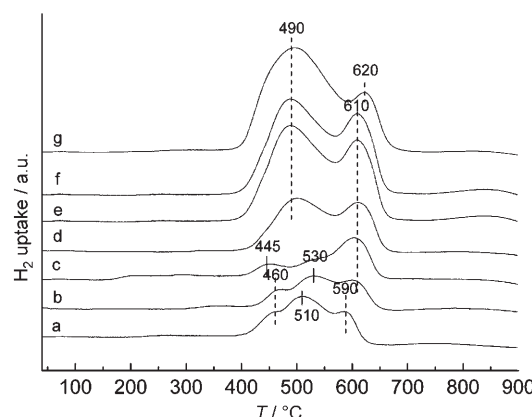

Figure 8. TPR patterns of catalysts a) **1**, b) **2**, c) **3**, d) **4**, e) **5**, f) **6**, and g) **7**.

shows the TPR profiles for the samples with different nickel contents. The H$_2$ TPR profile of Ni/SBA-15 powder was also measured for comparison (see Supporting Information). There are no clear reduction peaks for the FeCrAl alloy foil and SBA-15 in the temperature range 25–900 °C, whereas the TPR profiles are different for the Ni/SBA-15/Al$_2$O$_3$/FeCrAl catalysts. For catalyst **1**, three reduction peaks appear at 460 °C, 510 °C, and 590 °C; these temperatures are higher than those reported for pure NiO.[43] This may be caused by the reduction of NiO, which has a small interaction with the support. Upon increasing the nickel content to 3.5 % (**2**, Figure 8b), the reduction peaks at 510 °C and 590 °C shift to 530 °C and 610 °C, respectively. For the catalyst **3** (Figure 8c), the reduction peak at 460 °C shifts slightly to lower temperature (445 °C) whereas the other two reduction peaks are not shifted. With further increases in the nickel content from 5 % (**4**) to 12 % (**6**) (Figure 8 d–f), these peaks change significantly. The peak at 445 °C again shifts to higher temperature (490 °C), and the intensity of this peak increases also. However, the intensity of the peak at 610 °C decreases with increasing nickel content in the catalyst. At a nickel content of 16 % (**7**), the higher-temperature reduction peak appears at 620 °C (Figure 8g).

For the Ni/SBA-15 samples (see Supporting Information), except those with 3.0 % and 3.5 % Ni contents, there are only two reduction peaks. The low-temperature reduction peak appears at 471 °C, and the high-temperature reduction peak shifts from 658 °C to 697 °C with increasing nickel content. At the same time, the intensity of the two reduction peaks is a maximum with a nickel content of 16 % (Supporting Information). The Ni/SBA-15 with 3.0 % and 3.5 % Ni loadings display three reduction peaks at 471 °C, 532 °C, and 658 °C.

The reduction of supported nickel catalysts by TPR has been studied recently by a number of groups.[43, 44] Several reduction peaks are observed in the TPR profiles. As Ni^{II} is reduced to Ni^0 without going through intermediate oxides, the hydrogen consumption peaks appearing in different temperature regions have been assigned to the reduction of different species.[45] Generally, low-temperature peaks are attributed to the reduction of large NiO particles, while the peaks at higher temperature are attributed to the reduction of NiO in intimate contact with the oxide support.[46]

According to the above analysis, the reduction peaks appearing in the low-temperature region (400–550 °C) for both the Ni/SBA-15/Al$_2$O$_3$/FeCrAl and Ni/SBA-15 samples correspond to bulk NiO, which has a small interaction with the support, while the reduction peak at higher temperatures (550–700 °C) can be attributed to reduction of the fixed NiO, which has a stronger interaction with the support. The reduction peaks for Ni/SBA-15 samples with Ni loadings of 3.0% and 3.5% which appear at 471 °C (see Supporting Information) shift to lower temperature (460 °C, Figure 8) in the supported Ni/SBA-15/Al$_2$O$_3$/FeCrAl samples. However, the reduction peak at 471 °C for Ni/SBA-15 samples with over 4% nickel content (Supporting Information) shift to higher temperature (490 °C, Figure 8) in the supported Ni/SBA-15/Al$_2$O$_3$/FeCrAl samples. Note that the redox properties of NiO are modified as Ni/SBA-15 is supported on the Al$_2$O$_3$/FeCrAl support.

Upon increasing the Ni loading in Ni/SBA-15 samples, the intensity of the reduction peak in the low-temperature region (400–550 °C) increases sharply, as does the peak in the high-temperature region (550–700 °C). This indicates the presence of bulk NiO to an appreciable extent, which is confirmed by the XRD data of the Ni/SBA-15 samples (Figure 1b). As Ni/SBA-15 is supported on Al$_2$O$_3$/FeCrAl, the intensity and the H$_2$ consumption of the reduction peak in the high-temperature region (550–700 °C) decreases gradually, the reverse of the Ni/SBA-15 samples. At the same time, it can be concluded that NiO can be better dispersed as Ni/SBA-15 is supported on the Al$_2$O$_3$/FeCrAl support from the XRD profiles of the samples. Thus, it is expected that relatively small and finely dispersed Ni metal particles are obtained during reduction of the Ni/SBA-15/Al$_2$O$_3$/FeCrAl catalysts. In this case, the ensemble size on the metal surface becomes smaller, resulting in good coke resistance, as the ensemble size necessary for carbon formation is larger than that for methane reforming.[47] This phenomenon results in stable activity during methane reforming with CO$_2$ owing to the prevention of carbon formation from methane decomposition.

On the basis of the H$_2$ TPR results for the Ni/SBA-15/Al$_2$O$_3$/FeCrAl and Ni/SBA-15 samples, it can be deduced that there are strong interactions between NiO, SBA-15, and the Al$_2$O$_3$/FeCrAl support. The interaction changes the redox properties of the samples and influences the catalytic activity. Furthermore, the interaction affects the stability of the Ni/SBA-15/Al$_2$O$_3$/FeCrAl catalysts.

Conclusions

To summarize, monolithic Ni/SBA-15/Al$_2$O$_3$/FeCrAl catalysts were prepared. Their structures and properties were characterized, and their catalytic activity for methane reforming with CO$_2$ was evaluated. It can be concluded from the present results that in the Ni/SBA-15/Al$_2$O$_3$/FeCrAl catalysts, the phase structures are NiO, α-Al$_2$O$_3$, and γ-Al$_2$O$_3$. The hexagonal mesoporous structure of SBA-15 is still present in the Ni/SBA-15/Al$_2$O$_3$/FeCrAl catalysts, and the framework of SBA-15 has some constriction with increasing nickel content during the calcination procedure. The Ni/SBA-15/Al$_2$O$_3$/FeCrAl catalysts show ex-

cellent catalytic activity and stability in methane reforming with CO$_2$; after 1400 h reaction, the conversions of CH$_4$ and CO$_2$ are 90.6% and 91.0%, respectively, and the CO and H$_2$ selectivities are 92.3% and 93.6%, respectively. The mesoporous structure of SBA-15 can depress nickel sintering, which can accelerate formation of coke, and enhances the catalytic activity and stability. There is strong interaction between the NiO, SBA-15, and the Al$_2$O$_3$/FeCrAl support. The interaction significantly changes the redox properties and enhances the catalytic activity and stability of the Ni/SBA-15/Al$_2$O$_3$/FeCrAl catalysts.

Experimental Section

Catalyst Preparation

The FeCrAl alloy foils (OC404, Sandvik steel, Sweden) were first rolled into metallic supports, which were made up of several cylinders of different diameters and 50 mm in length. To remove the oil, the supports were cleaned in ethanol and then basic and acidic solution, respectively, then thoroughly rinsed in deionized water. Then, the surface-treated metallic supports were calcined at 950 °C for 15 h in air. A boehmite primer sol was used as first wash coat layer to improve the adhesion between the wash coat layers and the heat-treated metallic support. The heat-treated metallic supports were immersed in the sol, with a withdrawal velocity of 3 cm min^{-1} to ensure uniformity, then dried in air and thereafter at 120 °C for 3 h, and then calcined at 500 °C for 4 h to afford the monolithic support (Al$_2$O$_3$/FeCrAl). SBA-15 mesoporous material was prepared following the reported procedure.[48] Ni/SBA-15 samples were prepared by impregnating the SBA-15 support with different aqueous solutions of nickel nitrate at specific concentrations at room temperature overnight followed by calcinations at 500 °C for 4 h. The mass fraction of Ni in the Ni/SBA-15/Al$_2$O$_3$ sample was in the range of 3.0–16%. The monolithic supports were dipped into the slurry of the Ni/SBA-15 samples, withdrawn at a constant speed of 3 cm min^{-1}, dried in air and thereafter at 120 °C for 3 h, and then calcined at 500 °C for 4 h to afford the monolithic Ni/SBA-15/Al$_2$O$_3$/FeCrAl catalysts. The weight of Ni/SBA-15 is about 7 wt% in the monolithic catalyst.

Catalyst Characterization

X-ray powder diffraction (XRD) patterns were obtained on a Rigaku D/MAX2500 VB2+/PC diffractometer using CuKα radiation at 40 kV and 200 mA. Temperature-programmed reduction (TPR) experiments were performed using a Thermo Electron Corporation TPD/R/O 1100 series catalytic surface analyzer equipped with a TCD detector. The catalysts were preheated with 10% O$_2$/N$_2$ mixture at a rate of 20 °C min^{-1} up to 500 °C, then cooled in flowing N$_2$ to room temperature, and thereafter reduced with 5% H$_2$/N$_2$ mixture at a heating rate of 20 °C min^{-1} up to 900 °C. N$_2$ adsorption–desorption experiments were performed with a Quantachrome Autosorb-1 automatic surface area and pore size analyzer. The samples were pretreated at 300 °C for 4 h, and the specific surface areas of the samples were determined using the Brunauer–Emmett–Teller (BET) method. The pore volumes and pore size distributions were derived from the desorption profiles of the isotherms using the Barrett–Joyner–Halanda (BJH) method. The coating adherence was qualitatively measured by ultrasonic vibration test using a KQ-400 DB apparatus. The coated foils were immersed horizontally in deionized water inside a beaker and then treated in an ultrasonic bath for 20 min at 130 W to measure the weight loss

induced by exposure to ultrasonic vibration. The weight loss of both Al_2O_3 layers and Ni/SBA-15 layers was less than 3.5 wt%.

Catalytic Activity and Stability Tests

The catalytic activity of the catalysts was carried out in a tubular fixed-bed flow microreactor made of quartz (i.d. 6 mm; length 350 mm) under atmospheric pressure at 700–850 °C. The test was performed with cylindrical monolithic catalysts, which were made up of several cylinders in different diameter and 50 mm in length. Before reaction, the samples were reduced in hydrogen flow at 750 °C for 3.5 h and then cooled to 700 °C under Ar flow. A diluted reactant gas stream comprising methane (99.99% purity) and carbon dioxide (99.99% purity) with 1:1 CH_4/CO_2 molar ratio was introduced into the reactor. The range of gas hourly space velocities varied from 2000 to 6000 mL g^{-1} h^{-1}. The velocities of the reactant gases were controlled by two mass flow controllers (Seven Star D07). The reaction temperature was controlled with a thermocouple attached to the outer wall of the reactor at a position corresponding to the center of the catalytic bed, and the outlet products were analyzed by an online gas chromatography (Beijing East & West Electronics Institute, GC-4000 A) with a TCD detector. Kinetic studies were conducted with significantly low conversions, which were usually controlled to be significantly lower than those defined by thermodynamic equilibrium, by adjusting the gas hourly space velocity (54 000 mL g^{-1} h^{-1}). Rate limitation by external and/or internal mass transfer under differential conditions proved to negligible by applying suitable experimental criteria.

Acknowledgements

[1] E. Ruckenstein, Y. H. Hu, *Appl. Catal. A* **1995**, *133*, 149–161.

[2] S. Wang, G. Q. M. Lu, *Appl. Catal. B* **1998**, *16*, 269–277.

[3] V. R. Choudhary, B. S. Uphade, A. S. Mamman, *Appl. Catal. A* **1998**, *168*, 33–46.

[4] I. Istadi, N. A. S. Amin, *Fuel* **2006**, *85*, 577–592.

[5] J. A. Sullivan, J. A. Doherty, *Appl. Catal. B* **2005**, *55*, 185–194.

[6] K. Zhang, U. Kogelschatz, B. Eliasson, *Energy Fuels* **2001**, *15*, 395–402.

[7] J. H. Bitter, W. Hally, K. Seshan, J. G. van Ommen, J. A. Lercher, *Catal. Today* **1996**, *29*, 349–353.

[8] J. H. Bitter, K. Seshan, J. A. Lercher, *J. Catal.* **1998**, *176*, 93–101.

[9] S. Sharma, S. Hilaire, J. M. Vohs, R. J. Gorte, H. W. Jen, *J. Catal.* **2000**, *190*, 199–204.

[10] D. Dissanayake, M. P. Rosynek, K. C. C. Kharas, J. H. Lunsford, *J. Catal.* **1991**, *132*, 117–127.

[11] V. R. Choudhary, A. M. Rajput, B. Prabhakar, *J. Catal.* **1993**, *139*, 326–328.

[12] K. Tomishige, Y. Chen, K. Fujimoto, *J. Catal.* **1999**, *181*, 91–103.

[13] Y. W. Chen, W. J. Wang, *Catal. Lett.* **2000**, *71*, 41–46.

[14] C. Crisafulli, S. Scire, L. Solarino, *Appl. Catal. A* **2002**, *225*, 1–9.

[15] K. S. Hwang, H. Y. Zhu, G. Q. Lu, *Catal. Today* **2001**, *68*, 183–190.

[16] Y. H. Hu, E. Ruckenstein, *Adv. Catal.* **2004**, *48*, 297–345.

[17] Z. Y. Hou, O. Yokota, T. Tanaka, T. Yashima, *Catal. Lett.* **2003**, *89*, 121–127.

[18] Z. Y. Hou, T. Yashima, *Appl. Catal. A* **2004**, *261*, 205–209.

[19] J. M. Wei, B. Q. Xu, J. L. Li, Z. X. Cheng, Q. M. Zhu, *Appl. Catal. A* **2000**, *196*, L167–L172.

[20] M. A. Ermakova, D. Y. Ermakov, G. Kuvshinov, *Appl. Catal. A* **2000**, *201*, 61–70.

[21] B. S. Liu, C. T. Au, *Appl. Catal. A* **2003**, *244*, 181–195.

[22] K. Takehira, T. Shishido, P. Wang, T. Kosaka, K. Takaki, *J. Catal.* **2004**, *221*, 43–54.

[23] M. C. J. Bradford, M. A. Vannice, *Appl. Catal. A* **1996**, *142*, 73–96.

[24] V. R. Choudhary, A. S. Mamman, *Appl. Energy* **2000**, *66*, 161–175.

[25] M. L. Zhang, S. F. Ji, L. H. Hu, F. X. Yin, C. Y. Li, H. Liu, *Chin. J. Catal.* **2006**, *27*, 777–782.

[26] F. X. Yin, S. F. Ji, B. H. Chen, L. P. Zhao, H. Liu, C. Y. Li, *Appl. Catal. B* **2006**, *66*, 265–273.

[27] E. Włoch, A. Łukaszczyk, Z. Żurek, B. Sulikowski, *Catal. Today* **2006**, *114*, 231–236.

[28] Z. Y. Hou, T. Yashima, *Appl. Catal. A* **2004**, *261*, 205–209.

[29] S. Roy, A. K. Heibel, W. Liu, T. Boger, *Chem. Eng. Sci.* **2004**, *59*, 957–966.

[30] G. Groppi, W. Ibashi, E. Tronconi, P. Forzatti, *Chem. Eng. J.* **2001**, *82*, 57–71.

[31] X. D. Wu, D. Weng, S. Zhao, *Surf. Coat. Technol.* **2005**, *190*, 434–439.

[32] S. Zhao, J. Z. Zhang, D. Weng, X. D. Wu, *Surf. Coat. Technol.* **2003**, *167*, 97–105.

[33] F. X. Yin, S. F. Ji, N. Z. Chen, M. L. Zhang, L. P. Zhao, C. Y. Li, H. Liu, *Catal. Today* **2005**, *105*, 372–377.

[34] F. X. Yin, S. F. Ji, B. H. Chen, Z. L. Zhou, H. Liu, C. Y. Li, *Appl. Catal. A* **2006**, *310*, 164–173.

[35] Y. Park, T. Kang, J. Lee, P. Kim, H. Kim, J. Yi, *Catal. Today* **2004**, *97*, 195–203.

[36] Y. M. Liu, Y. Cao, S. R. Yan, W. L. Dai, K. N. Fan, *Catal. Lett.* **2003**, *88*, 61–67.

[37] Q. H. Zhang, Y. Wang, Y. Ohishi, T. Shishido, K. Takehira1, *J. Catal.* **2001**, *202*, 308–318.

[38] Z. F. Yan, R. G. Ding, L. H. Song, L. Qian, *Energy Fuels* **1998**, *12*, 1114–1120.

[39] J. M. Wei, B. Q. Xu, J. L. Li, Z. X. Cheng, Q. M. Zhu, *Appl. Catal. A* **2000**, *196*, L167–L172.

[40] M. C. Bradford, M. A. Vannice, *Appl. Catal.* **1996**, *142*, 97–122.

[41] Y. Matsumura, T. Nakamori, *Appl. Catal. A* **2004**, *258*, 107–114.

[42] M. Kruk, M. Jaroniec, *Chem. Mater.* **2001**, *13*, 3169–3183.

[43] B. Scheffer, P. Molhoek, J. A. Moulijn, *Appl. Catal.* **1989**, *46*, 11–30.

[44] C. Louis, Z. X. Cheng, M. Che, *J. Phys. Chem.* **1993**, *97*, 5703–5712.

[45] R. Molina, G. Poncelet, *J. Catal.* **1998**, *173*, 257–267.

[46] A. M. Diskin, R. H. Cunningham, R. M. Ormerod, *Catal. Today* **1998**, *46*, 147–154.

[47] J. R. Rostrup-Nielsen, *Stud. Surf. Sci. Catal.* **1991**, *68*, 85–88.

[48] D. Y. Zhao, J. L. Feng, Q. S. Huo, N. Melosh, G. H. Fredrickson, B. F. Chmelka, G. D. Stucky, *Science* **1998**, *279*, 548–552.